Supporting Information

Structural and Electronic Studies of Metal Carbide Clusterfullerene $Sc_2C_2@C_s$-C_{72}

Yongqiang Feng, Taishan Wang,*, Jingyi Wu, Lai Feng,* Junfeng Xiang, Yihan Ma, Zhuxia Zhang, Li Jiang, Chunying Shu, and Chunru Wang*

Contents

Experimental Section:

1. The synthesis and purification of $Sc_2C_2@C_{72}$-C_s

Graphite rods were core-drilled and subsequently packed with a mixture of Sc/Ni_2 alloy and graphite powder in a weight ratio of 2:1. These rods were then vaporized in a Krätschmer-Huffman generator at 200 Torr He. The resulting soot was Soxlet-extracted with toluene for 24 h. $Sc_2C_2@C_{72}$-C_s was isolated from various empty fullerenes and other scandium metallofullerenes by HPLC.

2. HPLC data of purified $Sc_2C_2@C_{72}$-C_s

The stage 1 and 2 separations were repeated several times to obtain purified $Sc_2C_2@C_{72}$-C_s. Figure S3 and Figure S4 show the HPLC data of purified $Sc_2C_2@C_{72}$-C_s with Buckyprep and Buckyprep-M columns. These HPLC analyses also confirm the purity of $Sc_2C_2@C_{72}$-C_s.

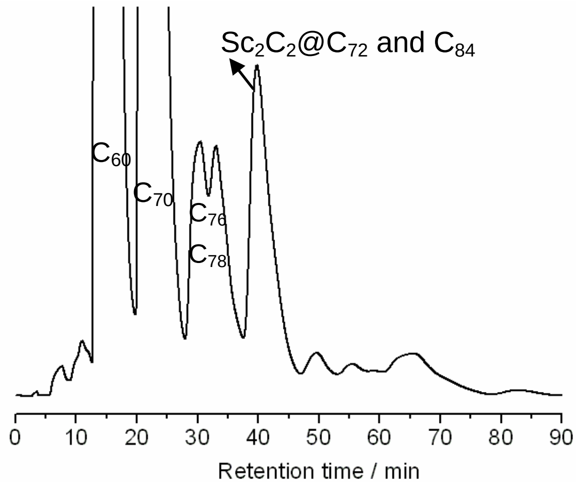

Figure S1. The first stage HPLC profile of toluene extract of the soot containing scandium endohedral metallofullerenes (20×250 mm Buckyprep column; flow rate 12 mL/min; toluene as eluent).

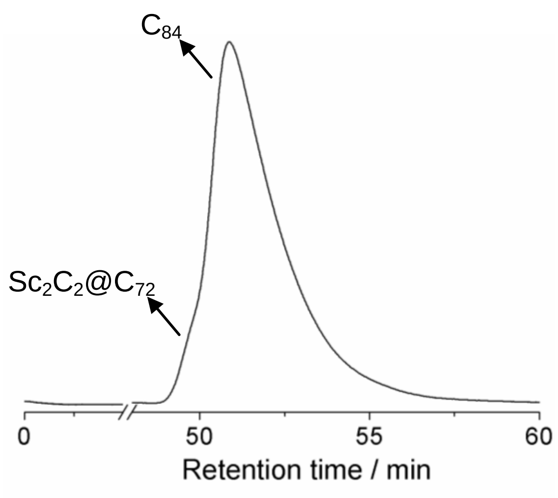

Figure S2. The second stage HPLC profile of C_{84} and $Sc_2C_2@C_{72}$-C_s fullerenes (20×250 mm Buckyprep column; flow rate 9 mL/min; toluene as eluent).

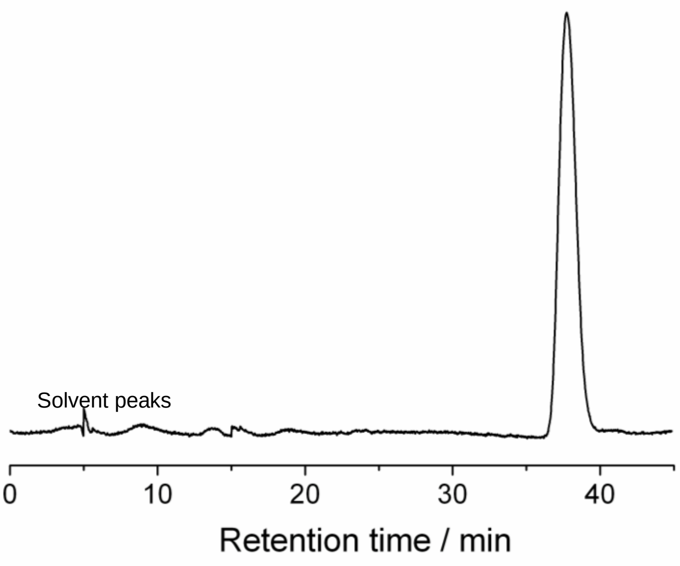

Figure S3. Chromatogram of the isolated $Sc_2C_2@C_{72}$-C_s (20×250 mm Buckyprep column; flow rate 12 mL/min; toluene as eluent).

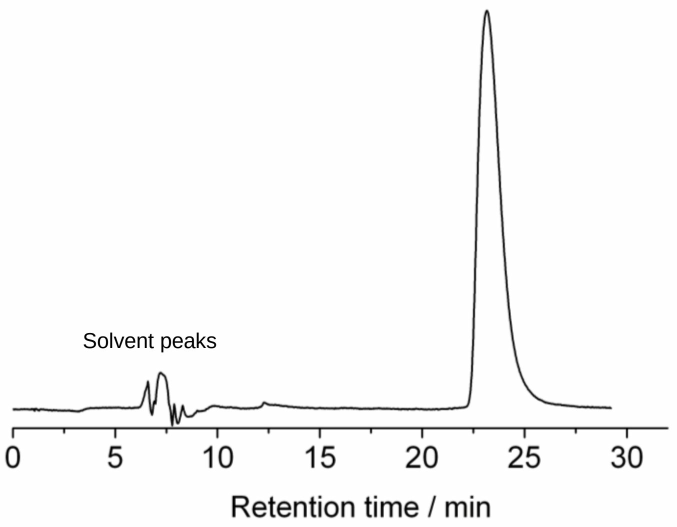

Figure S4. Chromatogram of the isolated $Sc_2C_2@C_{72}$-C_s (20×250 mm Buckyprep-M column; flow rate 12 mL/min; toluene as eluent).

3. MALDI-TOF mass spectrum of purified $Sc_2C_2@C_{72}$-C_s

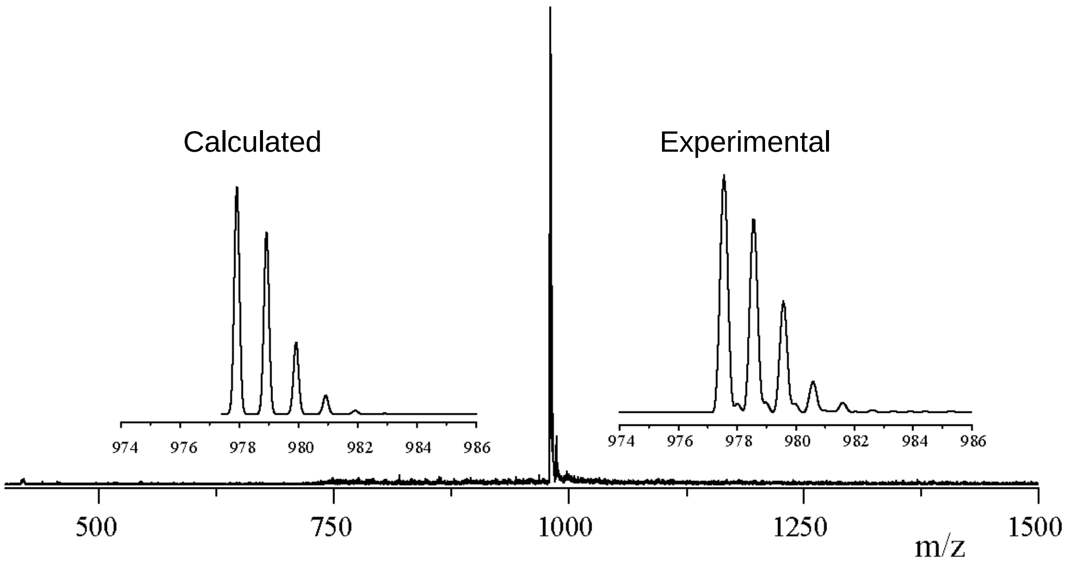

Figure S5. MALDI-TOF mass spectrum of pure $Sc_2C_2@C_{72}$-C_s. The insets show the experimental and calculated isotope distributions of $Sc_2C_2@C_{72}$-C_s.

4. UV/Vis-NIR spectrum of purified $Sc_2C_2@C_{72}$-C_s

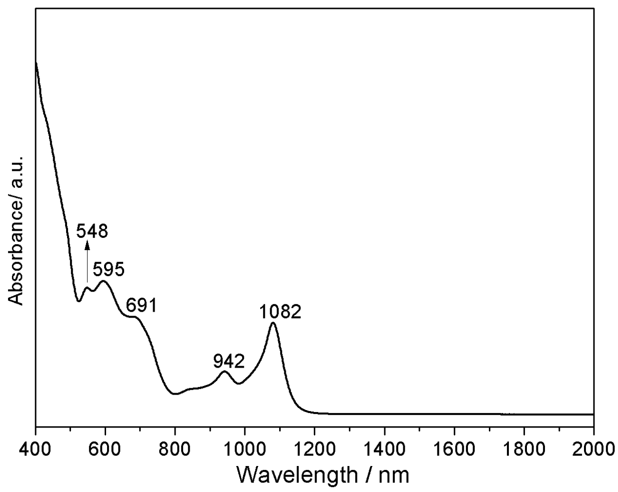

Figure S6. UV/Vis-NIR spectrum of purified $Sc_2C_2@C_{72}$-C_s in CS_2.

The UV/vis−NIR absorption spectrum of $Sc_2C_2@C_s$-C_{72} is shown in Figure S5, displaying five obvious absorption peaks at 548, 595, 691, 942, and 1082 nm. Such spectral pattern is similar to that of $Sc_2S@C_s$-C_{72}, in which absorption peaks were observed at 432, 535, 583, 678, 939, and

1076 nm[S1]. All the featured absorptions of these two species are listed in Table 1. It is well known that the absorptions of metallofullerenes are mainly due to the π-π* transitions, which are characteristic of the symmetry as well as the electronic structure of the fullerene cage.[S2] The absorption differences between $Sc_2C_2@C_s$-C_{72} and $Sc_2S@C_s$-C_{72} can be attributed to the different motional behaviors of endohedral clusters or to the different contributions of $(C_2)^{2-}$ and S^{2-} units, which might impose different influence on the cage symmetries and electronic structures of fullerenes. Moreover, for $Sc_2C_2@C_s$-C_{72}, the spectral onset of 1224 nm corresponds to a band gap of 1.01 eV. As for $Sc_2S@C_s$-C_{72}, the spectral onset is 1192 nm, suggesting a band gap of 1.04 eV.

Table S1. UV/vis−NIR absorptions of $Sc_2C_2@C_s$-C_{72} and $Sc_2S@C_s$-C_{72}.

compound	absorption peaks (nm)				
$Sc_2C_2@C_s$-C_{72}	548	595	691	942	1082
$Sc_2S@C_s$-C_{72}[S1]	535	583	678	939	1076

5. CV measurement of $Sc_2C_2@C_s(10528)$-C_{72}

Electrochemistry experiments were carried out in *o*-DCB solvent (0.05 M $(n\text{-}Bu)_4NPF_6$, scan rate, 100 mV s^{-1}) with glassy carbon as the working, Pt wire and Ag wire as the counter and reference electrodes, respectively. The potentials were referred to the $E_{1/2}$ value of the Fc/Fc^+ redox couple measured in the sample solution.

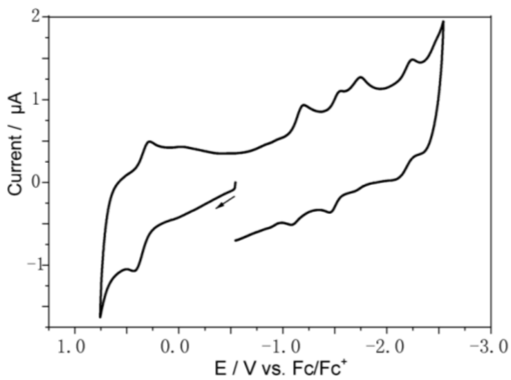

Figure S7. Cyclic voltammetry profile of $Sc_2C_2@C_s(10528)$-C_{72} in *o*-DCB. Scan rate, 100 mV s^{-1}.

6. ^{45}Sc NMR spectrum of $Sc_2C_2@C_s(10528)$-C_{72}

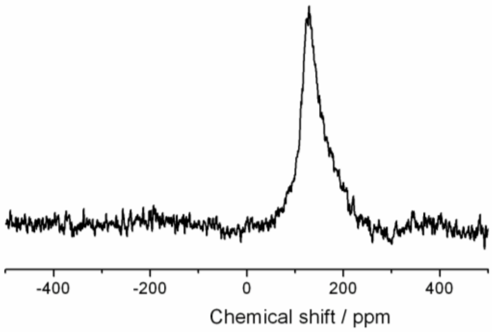

Figure S8. Experimental ^{45}Sc NMR spectrum (CS_2, 145 MHz) of $Sc_2C_2@C_s$-C_{72}.

7. X-ray structure of $Sc_2C_2@C_s(10528)$-C_{72}

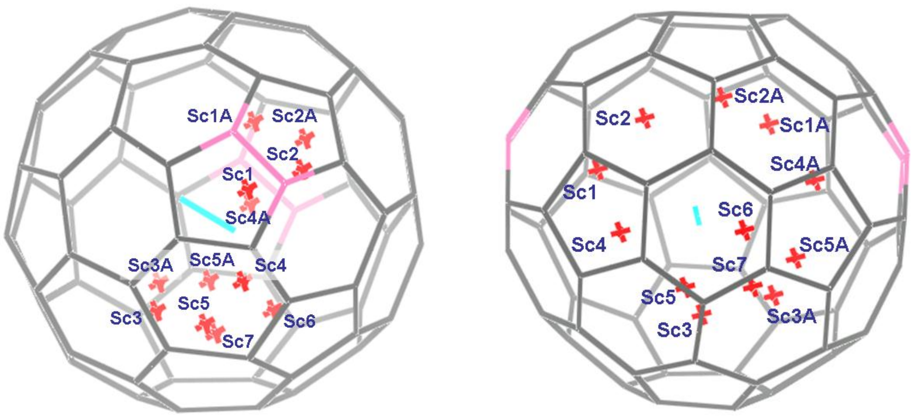

Figure S9. Two views of X-ray structure of $Sc_2C_2@C_s(10528)$-C_{72}, showing the distribution of disordered Sc positions. Those Sc sites labeled "A" are generated by the crystallographic mirror plane. Occupancies for these Sc positions are: Sc1, 0.249; Sc2, 0.212; Sc3, 0.190; Sc4, 0.143; Sc5, 0.127; Sc6, 0.094; Sc7, 0.061.

Calculation Section:

1. DFT calculated structure of Sc_2C_2@C_{72}-$\boldsymbol{C_s}$

Density functional theory (DFT) calculations were preformed to study the geometric structure of Sc_2C_2@C_{72}-C_s at GGA-PBE/DNP[S3] level by using the Dmol^3 code[S4, S5].

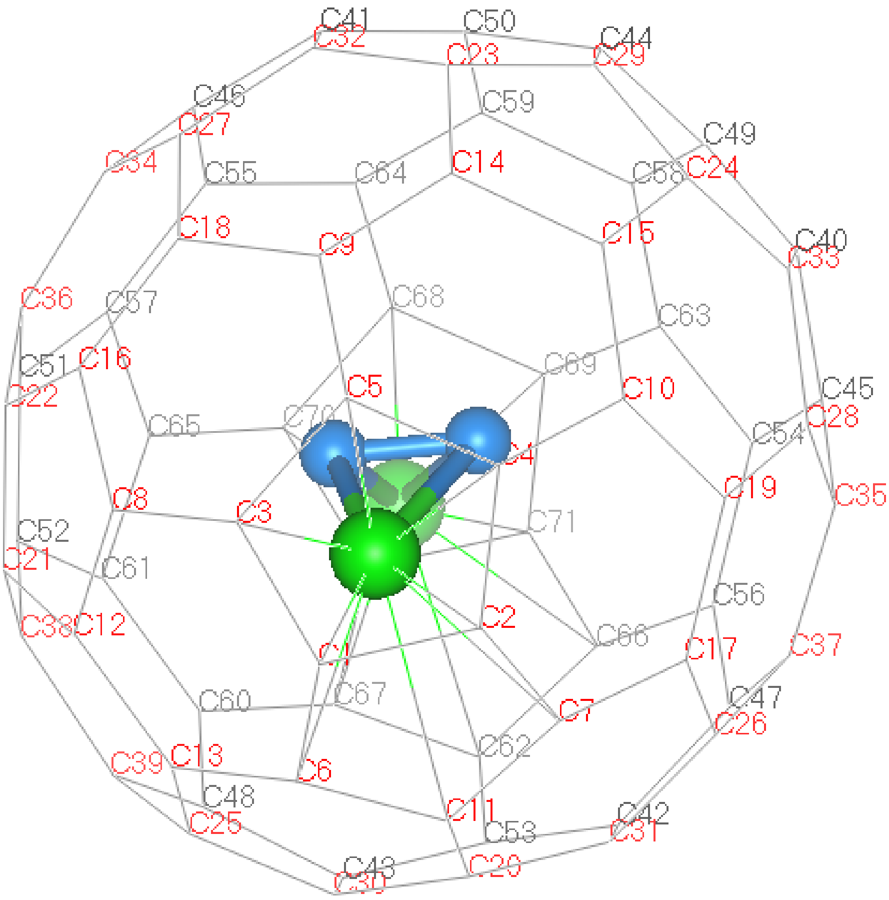

Figure S10. Optimized structure of Sc_2C_2@C_{72}-C_s.

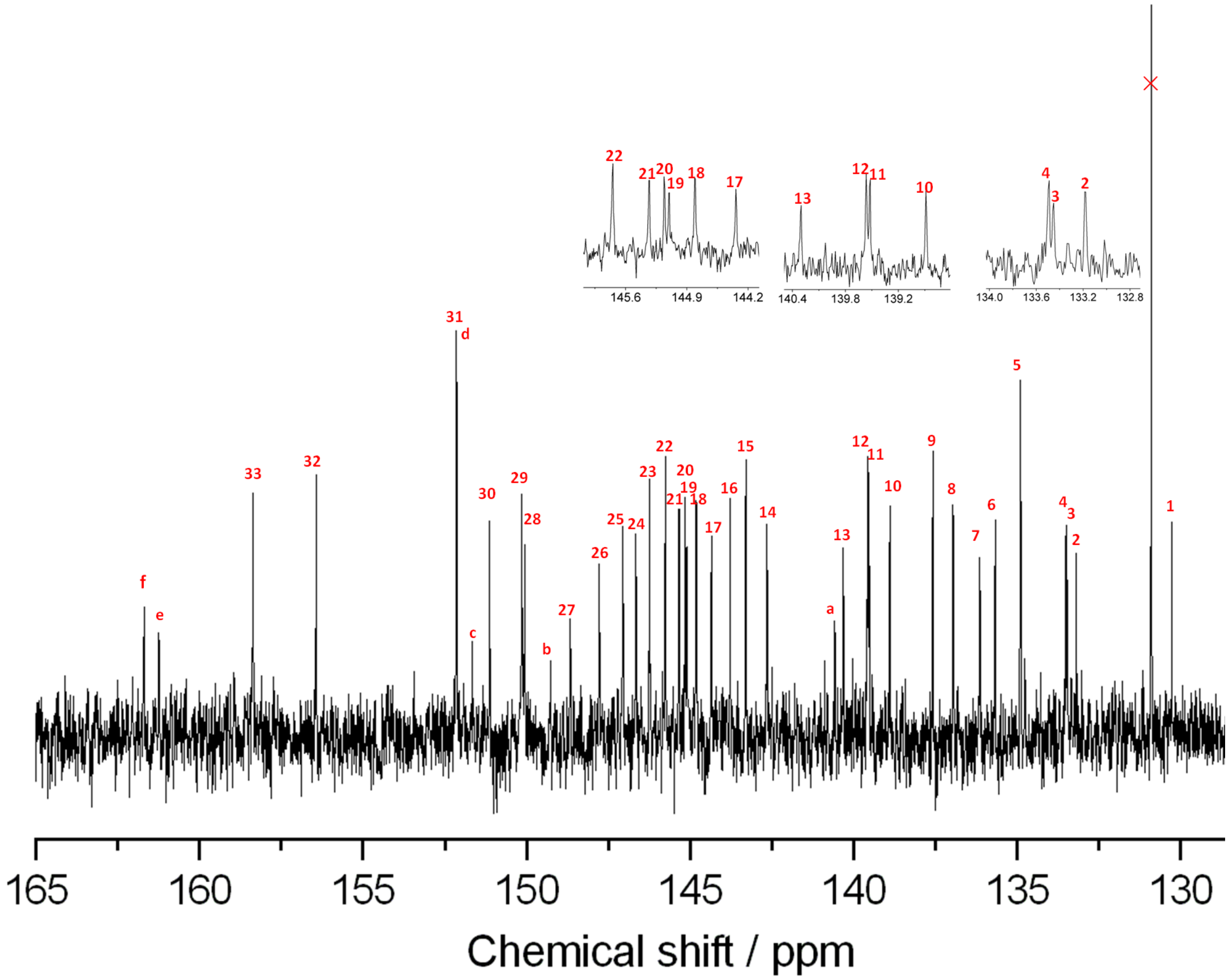

Figure S11. Experimental ^{13}C NMR Chemical Shifts for $Sc_2C_2@C_{72}$-C_s. 33 signals with full intensity and six signals with half intensity are marked with Arabic numerals and letters, respectively.

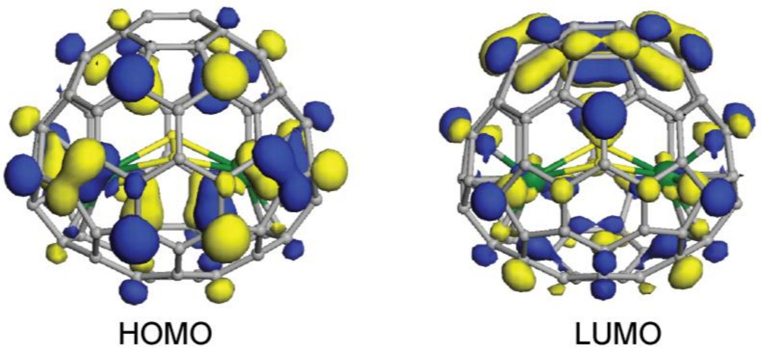

Figure S12. DFT calculated isodensity surface plots for the HOMO and LUMO of $Sc_2C_2@C_s(10528)$-C_{72}.

Table S2. Experimental and Calculated ^{13}C NMR Chemical Shifts for $Sc_2C_2@C_{72}$-C_s.

Site	Calculated δ (ppm)	Experimental δ (ppm)	Intensity
35-C	163.7024	161.69	1
34-C	162.5013	161.25	1
39-C	152.0877	152.14	(overlapped with 1,72-C)
38-C	150.6507	151.67	1
37-C	149.568	149.26	1
36-C	143.7849	140.56	1
29-C, 44-C	157.7987	158.37	2
22-C, 51-C	155.1819	156.43	2
1-C, 72-C	152.6885	152.14	(overlapped with 39-C)
26-C, 47-C	151.2228	151.13	2
28-C, 45-C	150.8183	150.15	2
14-C, 59-C	149.1547	150.05	2
2-C, 71-C	147.7982	148.66	2
21-C, 52-C	147.4193	147.77	2
30-C, 43-C	147.2213	147.04	2
15-C, 58-C	146.9127	146.65	2
25-C, 48-C	145.3566	146.23	2
18-C, 55-C	144.8773	145.75	2
31-C, 42-C	144.8033	145.33	2
27-C, 46-C	144.6006	145.16	2
6-C, 67-C	144.5249	145.10	2
23-C, 50-C	144.1111	144.81	2
32-C, 41-C	144.1108	144.34	2
33-C, 40-C	143.9319	143.77	2
3-C, 70-C	143.081	143.29	2
11-C, 62-C	142.7931	142.64	2
19-C, 54-C	140.9732	140.30	2
7-C, 66-C	139.9188	139.56	2
24-C, 49-C	139.7119	139.52	2
20-C, 53-C	138.9339	138.89	2
16-C, 57-C	137.2097	137.57	2
9-C, 64-C	136.1229	136.95	2
4-C, 69-C	135.9673	136.13	2
13-C, 60-C	135.4612	135.66	2
8-C, 65-C	135.0854	134.89	2
17-C, 56-C	134.4886	133.49	2
12-C, 61-C	134.2862	133.45	2
5-C, 68-C	134.23	133.19	2
10-C, 63-C	130.5157	130.26	2

Cartesian coordinates of $Sc_2C_2@C_{72}$-C_s predicted at the PBE/DNP level of theory:

C	1.034995	-0.993198	-4.181923
C	-0.388104	-1.242047	-4.114364
C	1.232105	0.435459	-4.037446
C	-1.080023	0.002705	-3.923640
C	-0.077390	1.063310	-3.894953
C	1.696811	-1.931290	-3.287857
C	-0.636249	-2.335623	-3.209860
C	2.266695	0.888227	-3.168902
C	-0.270988	2.254139	-3.095285
C	-2.249836	0.059874	-3.083938
C	0.657336	-2.803825	-2.735366
C	3.076307	-0.055117	-2.414198
C	2.743573	-1.461473	-2.398597
C	-1.586053	2.438278	-2.594715
C	-2.561643	1.355252	-2.583193
C	2.125601	2.092984	-2.397428
C	-1.790861	-2.332115	-2.348061
C	0.875096	2.807539	-2.353934
C	-2.666332	-1.142966	-2.331904
C	0.791048	-3.427188	-1.443664
C	3.528728	0.625487	-1.226258
C	2.951558	1.946451	-1.226312
C	-1.822551	3.246148	-1.421825
C	-3.385010	1.518919	-1.416403
C	2.927601	-2.159508	-1.160063
C	-1.674980	-3.131224	-1.171760
C	0.613528	3.559392	-1.174879
C	-3.479335	-0.935856	-1.181759
C	-2.940681	2.696333	-0.700858
C	1.999702	-3.175778	-0.716386
C	-0.410820	-3.675299	-0.723177
C	-0.734400	3.783488	-0.723356
C	-3.823958	0.387173	-0.726730
C	1.446517	3.424572	0.000000
C	-3.326937	-1.752535	0.000000
C	2.597843	2.587429	0.000000
C	-2.441129	-2.823153	0.000000
C	3.719856	-0.084752	0.000000
C	3.456871	-1.498300	0.000000
C	-3.823958	0.387173	0.726730
C	-0.734400	3.783488	0.723356
C	-0.410820	-3.675299	0.723177
C	1.999702	-3.175778	0.716386

C	-2.940681	2.696333	0.700858
C	-3.479335	-0.935856	1.181759
C	0.613528	3.559392	1.174879
C	-1.674980	-3.131224	1.171760
C	2.927601	-2.159508	1.160063
C	-3.385010	1.518919	1.416403
C	-1.822551	3.246148	1.421825
C	2.951558	1.946451	1.226312
C	3.528728	0.625487	1.226258
C	0.791048	-3.427188	1.443664
C	-2.666332	-1.142966	2.331904
C	0.875096	2.807539	2.353934
C	-1.790861	-2.332115	2.348061
C	2.125601	2.092984	2.397428
C	-2.561643	1.355252	2.583193
C	-1.586053	2.438278	2.594715
C	2.743573	-1.461473	2.398597
C	3.076307	-0.055117	2.414198
C	0.657336	-2.803825	2.735366
C	-2.249836	0.059874	3.083938
C	-0.270988	2.254139	3.095285
C	2.266695	0.888227	3.168902
C	-0.636249	-2.335623	3.209860
C	1.696811	-1.931290	3.287857
C	-0.077390	1.063310	3.894953
C	-1.080023	0.002705	3.923640
C	1.232105	0.435459	4.037446
C	-0.388104	-1.242047	4.114364
C	1.034995	-0.993198	4.181923
Sc	0.381634	-0.444787	-2.087720
Sc	0.381634	-0.444787	2.087720
C	-0.655833	-0.029926	0.000000
C	0.556609	0.348943	0.000000

References

S1 N. Chen, C. M. Beavers, M. Mulet-Gas, A. Rodríguez-Fortea, E. J. Munoz, Y.-Y. Li, M. M. Olmstead, A. L. Balch, J. M. Poblet and L. Echegoyen, *J. Am. Chem. Soc.*, 2012, **134**, 7851-7860.

S2 H. Shinohara, *Rep. Prog. Phy*, 2000, **63**, 843.

S3. J. P. Perdew, K. Burke and M. Ernzerhof, *Phys. Rev. Lett.* 1996, **77**, 3865-3868.

S4. B. Delley, *J. Chem. Phys.* 1990, **92**, 508-517.

S5. B. Delley, *J. Chem. Phys.* 2000, **113**, 7756. DMol3 is available as part of Material Studio.